NWRI CONTRIBUTION 86-110
Donelan (41)

This manuscript has been submitted to
the International Geoscience & Remote Sensing Symposium '86
Zurich, Switzerland, 8-11 September 1986
and the contents are subject to change.

A TWO-SCALE BRAGG SCATTERING MODEL FOR MICROWAVE BACKSCATTER FROM WIND GENERATED WAVES

by

[1] Mark A. Donelan[1] and [2]Willard J. Pierson, Jr.

[2]The City College of New York
New York, NY, USA

[1]Shore Processes Section
Hydraulics Division
National Water Research Institute
Canada Centre for Inland Waters
Burlington, Ontario, Canada

June 1986

MANAGEMENT PERSPECTIVE

This paper and the companion paper (Verification Results for a Two-Scale Model of Microwave Backscatter from the Sea Surface, Pierson and Donelan), present a new model for measuring winds over the ocean using satellite borne radar and present a preliminary verification of the model. These works respresent an important advance in our ability to measure wind speed and direction in a synoptic sense over the world's oceans. This in turn is a necessary step in improving weather forecasting. The model will likely be used in future weather satellites.

T. Milne Dick
Chief
Hydraulics Division

PERSPECTIVE DE GESTION

La présente communication et celle qui l'accompagne (Verification Results for a Two-Scale Model of Microwave Backscatter from the Sea Surface, Pierson et Donelan) décrivent un nouveau modèle de mesure des vents au-dessus des océans à l'aide d'un radar spatial et font état d'une vérification préliminaire du modèle. Ces travaux font progresser de façon importante notre capacité de mesurer à l'échelle synoptique la vitesse et la direction des vents au-dessus des océans du monde, ce qui est indispensable pour améliorer la prévision météorologique. Le modèle sera vraisemblablement utilisé dans de futurs satellites météorologiques.

Le chef,

T. Milne Dick
Division de l'hydraulique

RÉSUMÉ

Un nouveau modèle d'établissement du spectre des nombres d'onde pour mers entièrement formées est élaboré en fonction du gradient du vent moyen. La partie supérieure du spectre, qui définit les nombres d'onde de Bragg, est un spectre d'équilibre, en équilibre avec un terme de force du vent déterminé par $((U(\pi/k/C(k))-1)^2$, la dissipation visqueuse, qui est fortement fonction de la température de l'eau, et la dissipation par déferlement et microdéferlement. La partie inférieure du spectre, établie à partir d'observations de la hauteur des ondes de gravité, est unie à la partie supérieure. Divers paramètres sont ensuite ajustés aux données de vol du cercle de Tangley de l'AAFE pour la bande K_u. Le spectre complet sert alors dans la théorie de diffusion à double échelle de Bragg, avec réflexion spéculaire, à calculer la rétro-diffusion en fonction de la vitesse du vent, de sa direction et de son angle d'incidence ainsi que de la température de l'eau (qui détermine la viscosité) pour la bande K_u.

Mots clés : diffusion de Bragg, équilibre spectral, gammes d'équilibre, scattérométrie

A TWO-SCALE BRAGG SCATTERING MODEL FOR MICROWAVE BACKSCATTER FROM WIND GENERATED WAVES

Mark A. Donelan

National Water Research Institute
Burlington, Ontario, Canada

Willard J. Pierson, Jr.

The City College of New York
New York, NY, U.S.A.

ABSTRACT

A new model for the wavenumber spectrum for fully developed seas is derived as a function of the mean wind gradient. The high wavenumber part of the spectrum, which defines the Bragg wavenumbers, is an equilibrium spectrum in balance by a wind forcing term determined by $((U(\pi/k)/C(k))-1)^2$, viscous dissipation, which is a strong function of water temperature, and dissipation by breaking and microbreaking. The low wavenumber spectrum, constructed from surface elevation observations of gravity waves, is merged with the high wavenumber spectrum. Various parameters are adjusted to fit the AAFE Langley circle flight data for K_u-band. The full spectrum is then used in the two-scale Bragg scattering theory, plus specular reflection, to compute backscatter as a function of wind speed, direction, incidence angle, and water temperature (which determines viscosity) for K_u-band.

Keywords: Bragg scattering, spectral balance, equilibrium ranges, scatterometry.

1. INTRODUCTION

Donelan and Pierson (Ref. 6) (see also Pierson et al., Ref. 18) demonstrate that the wind parameter most closely related to microwave Bragg scattering is the wind very near the surface at a height of order of the wavelength of the Bragg resonant water wave. Frequency spectra of gravity waves (wavelength λ = 20.7 cm) were used to support the analysis. The results are of value in the interpretation of L-band synthetic aperature data. Neither wind speed $\bar{U}(19.5)$, nor friction velocity, u_*, is uniquely related to the wave spectral density, $\Phi(\omega)$, when data for various states of wave development are considered. A closer relationship beween the normalized spectrum, $\Phi(\omega)\omega^5/g^2$ and $(((\bar{U}(\pi g/\omega^2))\omega/g)-1)$ was shown. This new approach has been used to develop a new model for radar backscatter in Donelan and Pierson (Ref. 7).

We obtained a theoretical form for the high wavenumber spectrum that requires some empircially determined constants. The theoretical equilibrium spectrum links the waves to the wind. This spectrum is included in a two-scale Bragg scattering model to relate backscattering cross-section first to the wave spectrum and then to the wind that generated the waves.

The low wavenumber (gravity wave) part of the spectrum is for a fully developed wind generated sea. It is used to calculate the required slope variances for a two-scale model.

Observational results on wave growth and physical reasoning lead to a form of the wavenumber spectrum for capillary-gravity waves (wavenumber $k = 2\pi/\lambda$ in the range 10^{-1} to 10^{+1} cm^{-1}) which is in accord with observations. The dependence of spectral density on surface wind is deduced and demonstrates that power law model functions are inadequate and will, when fitted to a mid-range of surface wind data, underestimate the wind speed at both low and high speeds (as illustrated in Ref. 17).

The predicted VV normalized backscattering cross-sections $\sigma^0_{VV}(\bar{U},\chi,\theta)$, are compared with the circle flight data from Schroeder et al. (Ref. 20). They yield the observed incidence angle, wind speed and direction dependence for vertical polarization, except for high incidence angles, for which relatively small effects of sharp wedges and breaking waves are required.

2. WIND FORCING

Various attempts have been made to estimate the wind input to waves by measuring the pressure at or near the surface. The growth rates have been studied by Snyder et al. (Ref. 21); Hsiao and Shemdin (Ref. 9); and Hasselmann et al. (Ref. 8) among others. In general the growth rates show a quadratic dependence on (U/C-1), which has the character of wind input due to form drag - an idea first expounded by Jeffreys (Refs. 10 and 11). If the mechanism of wind input to waves is indeed analogous to form drag on a rough wall, then the appropriate reference wind is not that at the "critical height" (Miles, Ref. 15) but instead at some height above the roughness elements that is related to their scale. In a recent numerical calculation Al-Zanaidi and Hui (Ref. 1) obtain a result of the form of Eq. 1 but in which $U(\lambda)$ is used instead of $U(\lambda/2)$. The choice of wavelength related height cannot be specified by rigorous argument. In this paper, we have chosen one half wavelength as the reference height since at this height the disturbance due to a particular wavelength (observed to be exponential by Snyder et al., Ref. 21) has nearly vanished. $U(\lambda/2)$ is thus our reference wind or "U_∞" for the waves being considered. Note that $U(\lambda/2)$ is dependent on U(19.5) and the drag coefficient, which is taken

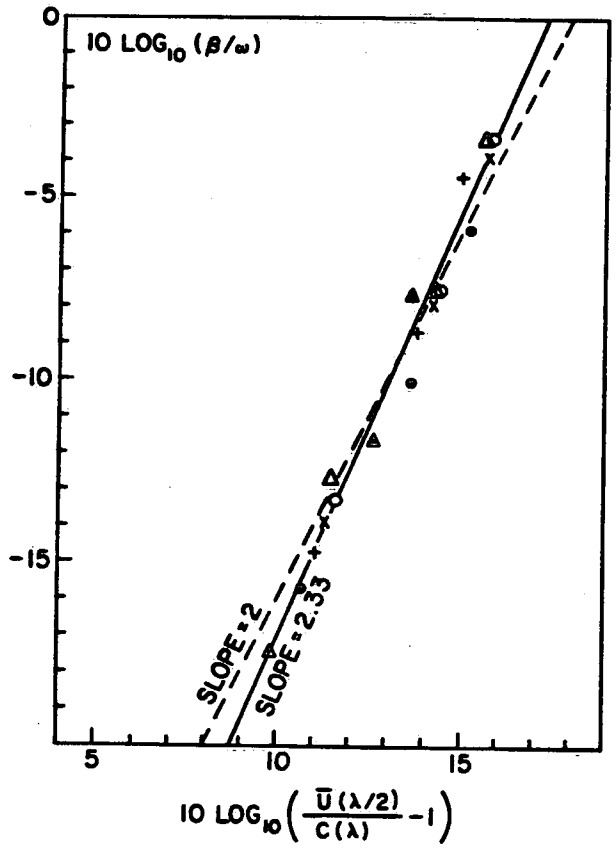

Figure 1. Normalized exponential growth rates versus $(\bar{U}(\lambda/2)/C(\lambda))-1$. The data are taken from Larson and Wright (Ref. 13) and the different symbols refer to different wavelengths (λ) of the growing water wave having phase speed $C(\lambda)$: 0.72 cm (▲); 1.25 cm (+); 1.85 cm (△); 2.72 cm (o); 4.05 cm (x); 6.98 cm (●) The dashed line corresponds to Eq. 1.

to be wind speed dependent as in Donelan (Ref. 3). (See also Ref. 17.)

Scatterometry is largely concerned with the capillary-gravity transition region of the spectrum where there have been no successful measurements of surface pressure and thereby estimates of direct wind forcing. However, Larson and Wright (Ref. 13), in a splendid experiment, obtained the exponential growth rates of capillary-gravity waves following an abruptly turned-on wind. The growth rates of these short waves have been analysed by Donelan and Pierson (Ref. 7) and found to correlate well with $(\bar{U}(\lambda/2)/C(\lambda))-1$ as shown in Figure 1. The correlation was considerably better than with u_*/c or $\bar{U}(19.5)/C$.

Therefore we take the wind forcing for short waves to be that suggested by the quadratic fit to the data of Larson and Wright (Figure 1).

$$\frac{\beta}{\omega}\frac{\rho_w}{\rho_a} = 0.194\left(\frac{\bar{U}(\lambda/2)}{C(\lambda)} - 1\right)^2 \qquad (1)$$

3. SPECTRAL BALANCE OF SHORT WAVES

For the high wavenumber part of the spectrum, sufficiently far from the spectral peak, the spectral balance may be dominated by wind input and dissipative processes - with other effects playing a lesser role.

The viscous dissipation of very short capillary waves has been worked out theoretically (Lamb, Ref. 12), and verified experimentally by Mitsuyasu and Honda (Ref. 16) among others. It is a function only of wavenumber, k and ν the kinematic water viscosity. The spectral decay rate through viscosity is $\beta_\nu = 4\nu k^2$.

The spilling of the crests of large gravity waves is clearly a major sink of wave energy. It depends strongly on spectral levels since no breaking occurs when the waves are not steep. A closer look at a wind driven sea reveals that the short gravity waves also break in a similar way, but the result is not spectacular and, without the production of foaming white caps, may even go unnoticed. The rate of dissipation of this "micro-breaking" is certainly dependent on spectral levels. Inasmuch as the dissipative region is locked to the wave crest and persists for a good fraction of a wave period, the energy loss is probably concentrated around the wavenumber of the breaking wave. Capillary-gravity waves appear to lose energy through the production of even shorter ripples at their crests.

Although dissipation through wave breaking must depend to some extent on the spectral density elsewhere in the spectrum, in the equilibrium range the spectral levels in the vicinity of k scale with the level at k. This is particularly true for the case of full development being discussed here. Thus we define the normalized dissipation rate, β_d/ω in terms of the local wavenumber and spectral density:

$$\frac{\beta_d}{\omega} = f_1\left(\Phi(k,\bar{\chi}),\ k,\ \gamma,\ g\right) + \frac{\beta_\nu}{\omega} \qquad (2)$$

where $\Phi(k, \bar{\chi})$ is the polar wavenumber spectrum with $\chi = \bar{\chi}$ in the wind direction, γ is the surface tension/density ratio and g is the gravitational acceleration.

Thus on dimensional grounds

$$\frac{\beta_d}{\omega} = f_1\left(k^4\,\Phi(k,\bar{\chi});\ \frac{\gamma k^2}{g}\right) + \frac{\beta_\nu}{\omega} \qquad (3)$$

We adopt, for convenience, a power law behaviour for the function f_1 as in Eq. 4.

$$\frac{\beta_d}{\omega} = \alpha\left(k^4\,\Phi(k,\bar{\chi})\right)^n + \frac{4\nu k}{C} \qquad (4)$$

where $\alpha = f_2\left(\frac{\gamma k^2}{g}\right)$ and $n = f_3\left(\frac{\gamma k^2}{g}\right)$.

The values of α and n will depend on the nature of the breaking process. Long gravity waves lose energy largely by sudden breaking (generally "spilling" in deep water). These waves break as their height increases suddenly during their passage through a group of waves (Donelan et al., Ref. 5). Capillary-gravity waves, on the other hand, appear to lose much of their energy to even shorter ripples formed at their crests when they steepen sufficiently. Waves in the center of the capillary-gravity range ($\gamma k^2/g = 1$) are nearly non-dispersive compared to gravity waves so that phase and group velocities are nearly equal and any increase in the height of a particular wave occurs

through dynamic processes and not simply as a consequence of its passage through a group. Thus α and n may be quite different for these waves, which dissipate continuously, than for dispersive waves which grow (and break) suddenly as a kinematic consequence of their passage through a group ($\gamma k^2/g < 1$, gravity waves) or the passage of a group through them ($\gamma k^2/g > 1$, capillary waves). We assume, therefore that α and n attain the asymptotic values a_1, n_1 and α_2, n_2 according to whether the waves are strongly dispersive or nearly non-dispersive. For a given average energy density, the intensity of energy loss is dependent on the rate at which waves overtake groups or vice versa. We parameterize this in the following manner by Eqs. 5 and 6.

$$n = (n_1 - n_2)\left|2 - \frac{g + 3\gamma k^2}{g + \gamma k^2}\right|^b + n_2 \qquad (5)$$

$$\ln \alpha = (\ln \alpha_1 - \ln \alpha_2)\left|2 - \frac{g + 3\gamma k^2}{g + \gamma k^2}\right|^b + \ln \alpha_2 \qquad (6)$$

where n_1 and α_1 are determined from observations of gravity wave spectra and b, n_2 and α_2 are picked to yield the best fit to the observed backscatter at K_u-band.

4. EQUILIBRIUM RANGES

Equating input, Eq. 1 and dissipation, Eq. 4, we obtain an expression for the downwind spectrum of the short waves in the "equilibrium" range.

$$\Phi(k,\bar{\chi}) = k^{-4}\left[\frac{0.194}{\alpha}\frac{\rho_a}{\rho_w}\left(\frac{\bar{U}(\pi/k)}{C(k)} - 1\right)^2 - \frac{4\nu k}{\alpha C(k)}\right]^{1/n} \qquad (7)$$

$$= 0, \text{ if } \bar{U}(\pi/k) < C(k) \text{ or if } \left[\ \right] \leq 0$$

Here "equilibrium" is used formally to mean where wind input and dissipation are locally (with respect to wavenumber) balanced.

Eq. 7 represents a one-dimensional slice through the equilibrium wavenumber spectrum in polar form for waves travelling downwind in the direction, $\bar{\chi}$. The balance of wind input and dissipation in the wind direction gives Eq. 7 and describes the downwind spectral values. For waves travelling at off-wind angles to the wind direction, $\bar{\chi}$, the wind input term is often given as in Eq. 8.

$$\Phi(k,\chi) = k^{-4}\left[\frac{0.194}{\alpha}\frac{\rho_a}{\rho_w}\left(\frac{\bar{U}\cos(\chi - \bar{\chi})}{C} - 1\right)^2 - \frac{4\nu k}{\alpha C}\right]^{1/n} \qquad (8)$$

However, at large angles to the wind, the wind input decreases rapidly and a simple balance between wind input and dissipation according to Eq. 8 is not observed in the field. Normal to the wind direction wind input, in terms of a constant mean wind, vanishes but observations reveal significant energy density of the short waves. The natural variability of the wind direction spreads the angular range of wind input beyond that which would occur in a laboratory tank with a well defined wind direction. Nonlinear interactions among waves may also act to spread the energy beyond $\pm\pi/2$. To account for this, though not to explain it, we have assumed, as observed by Donelan et al. (Ref. 4) that the spectrum of the short waves spreads according to Eq. 9, which allows the choice of h_1 to fit the crosswind backscatter measurements.

The value of h_1 was chosen so that Eq. 9 and Eq. 8 agree at $\Phi(k,\chi) = 0.8\ \Phi(k,\bar{\chi})$. Once h_1 has been chosen the complete azimuthal and wavenumber behaviour of the spectrum is described by Eq. 9 where the downwind value, $\Phi(k,\bar{\chi})$ is given by Eq. 7. The decision to base the choice of h_1 on the 80% height of the spectrum was determined by comparison with the crosswind circle flight data.

$$\Phi(k,\chi) = \Phi(k,\bar{\chi})\cdot\operatorname{sech}^2(h_1(\chi - \bar{\chi})) \qquad (9)$$

5. A COMPOSITE DIVIDED SCALE MODEL

When a broad spectrum of waves exists the modulation of the Bragg scattering waves by the longer waves will alter the observed backscattered power. Thus, in order to interpret observed backscatter from a wind-generated sea, the spectrum, Eq. 9, by itself is not sufficient. We must construct a model that includes the effects of the rest of the spectrum on the resonant Bragg waves insofar as these longer waves tilt the Bragg scatterers and produce variations in their heights over different phases of the longer waves. Such models have been called composite models.

Valenzuela (Ref. 22) has reviewed composite models in which the wave spectrum is divided into short Bragg scattering waves and longer waves whose principal function is to tilt the surface. In these models, one is interested in the wavenumber spectrum of the short waves and the probability density of slopes of the longer waves.

The parameters of the longer scale gravity waves - the "tilting waves", for short - can be tied down by observational results. By contrast, the only directional information available in the capillary-gravity range comes from Bragg scattering measurements, which at steady-state are necessarily made in the presence of tilting waves. The effects of the tilting waves are sufficiently large that such observational results can only be used to infer the wavenumber spectrum of the Bragg waves through a model that includes the effects of the tilting of the Bragg waves. Composite divided scale models provide the simplest approach to account for such effects. The unknown parameters of the short wave spectrum may therefore be inferred by adjusting them to yield good agreement between the model and observations of radar backscattering cross-section.

To construct the full wavenumber spectrum we use the directional spectra observations of Donelan et al. (Ref. 4) in the wavenumber range from 0 to 10 k_p patched to Eq. 9 from 10 k_p to ∞; where p denotes the spectral peak. Leykin and Rozenberg (Ref. 14) also argue that the spectral slope transition from ω^{-4} to ω^{-5} occurs at about 3.2 ω_p which corresponds to 10 k_p. The larger the value of n_1 in Eq. 5 the closer the spectrum will be to k^{-4} (or ω^{-5}) but the results are not sensitive to the choice of n_1 for n_1 greater than about 5. Consequently we take $n_1 = 5$. Matching the observed spectra to Eq. 9 at 10 k_p requires that $\ln \alpha_1 = 22$. Comparison with the circle flight data (see below) yields $n_2 = 1.15$, $\ln \alpha_2 = 4.6$ and $b = 3$.

As in all two-scale theories, the full wavenumber spectrum must be divided in some logical way into that part that is needed only to determine the variances of the two components of the slope from

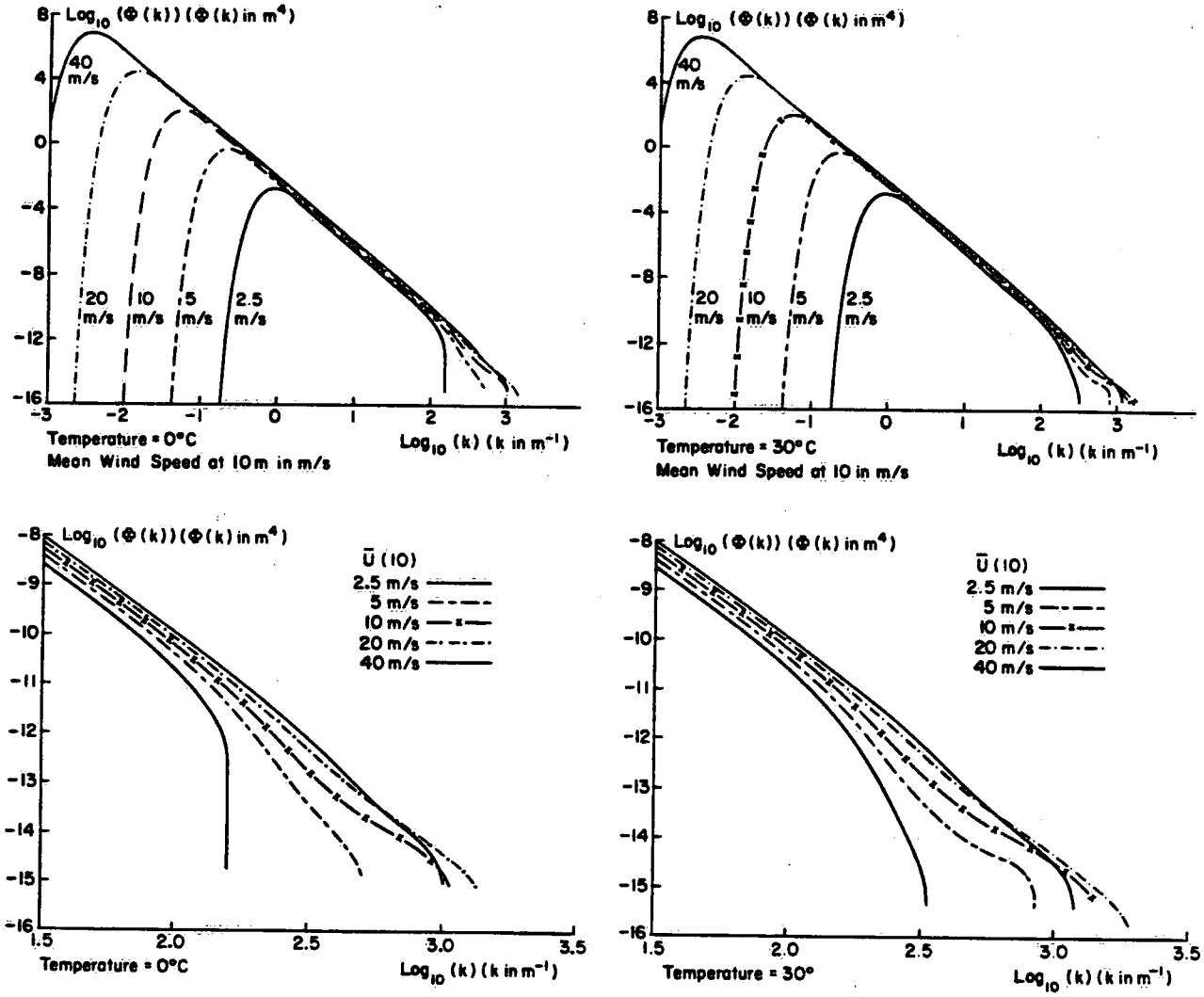

Figure 2. Sections through the wave number spectrum, $\Phi(k,\chi)$ in m^4 versus k in m^{-1}, at upwind for mean wind speeds at 10 m of 2.5, 5, 10, 20 and 40 m/s. Upper left, full spectrum for 0°C water temperature. Upper right, full spectrum for 30°C water temperature. Lower left, details of spectrum for 0°C for $\log_{10}k$ greater than 1.5. Lower right, details of spectrum for 30°C for $\log_{10}k$ greater than 1.5.

the low wavenumbers and that part that is kept to compute Bragg scattering from the shorter waves.

The description of the rationale behind such models in Valenzuela (Ref. 22) is helpful in this context. The patch of tilted sea surface covered by the Bragg waves must contain a sufficient number of these waves to produce some resonant backscatter. It also must be small enough so that the overall effect of variations in the slopes is not too greatly reduced by the application of what is effectively a low pass wavenumber filter to the full wavenumber spectrum. This is accomplished by an appropriate choice of $k_\Gamma (= k/\Gamma)$. This separation of scales factor, Γ, is the final parameter to be chosen for the Bragg scattering part of the model. The results are weakly dependent on the choice of Γ. By fitting the model to the circle flight data (Schroeder et al., Ref. 20), we have selected $\Gamma = 40$.

The composite spectra for $\chi = \bar{\chi}$ are shown in Figure 2 for various wind speeds and extreme values of water temperature of 0°C and 30°C. The two spectra for a wind of 40 m/s lie below portions of the spectra for 10 m/s and 20 m/s. As the wind at 10 m increases, the wind at π/k at first also increases, but eventually the rapidly increasing wind gradient (wind speed dependent drag coefficient) causes $\bar{U}(\pi/k)$ to decrease with increasing wind speed at 10 m. Increasing slopes of the tilting waves overcome this effect for some high winds, but eventually for high enough winds the Bragg backscatter will decrease.

These wavenumber spectra are then inserted into the two-scale backscatter theory given by Valenzuela (Ref. 22) to yield calculated normalized backscattering cross-sections for given wind speeds, wind directions, water temperatures and incidence angles.

Near normal incidence the wavelength of the Bragg wave rises sharply. However, Bragg scattering is not effective near nadir. We therefore impose a cut-off condition on the Bragg backscatter when the instantaneous incidence angle, $\theta_i < 18°$. The choice of 18° is made on the basis of the low incidence angle circle flight data.

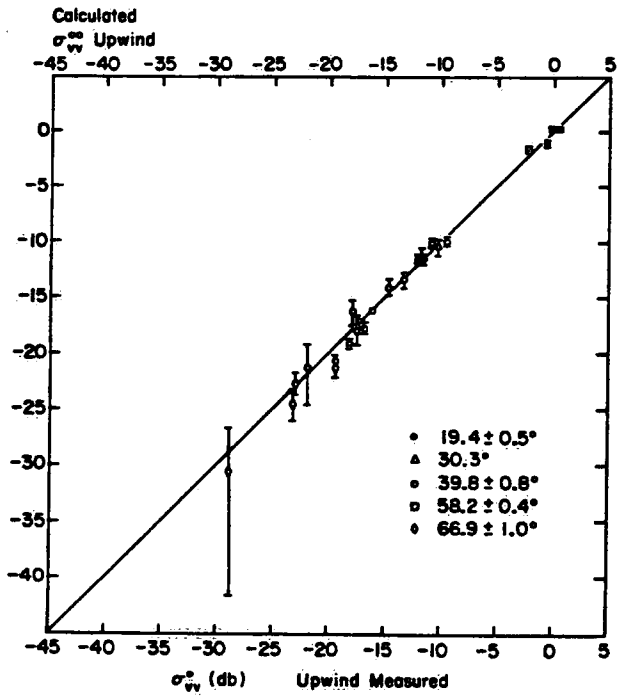

Figure 3. Measured vertically polarized backscatter values in db for upwind (abscissa) versus values calculated from the model (ordinate) for five incidence angles as coded. The line of perfect agreement is shown. The error bars are for plus and minus one m/s for the wind speed.

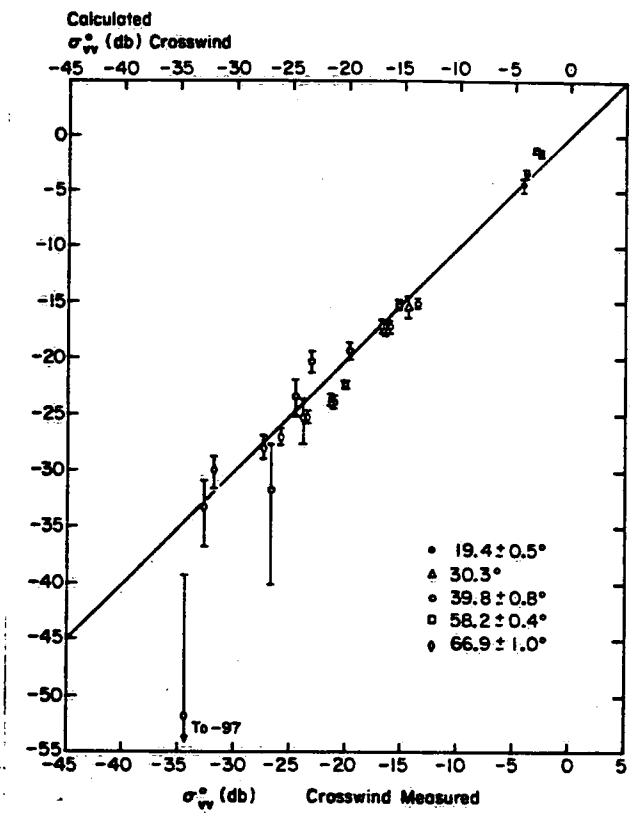

Figure 4. Same as Figure 3 except for crosswind.

Specular reflection contributes to the backscattered power particularly at low incidence angles such as 20°. The model includes a specular component in the manner described by Valenzuela (Ref. 22).

6. COMPARISON OF MODEL WITH CIRCLE FLIGHT DATA

The data used for parameter tuning and preliminary verification of the model are subsets of the AAFE Langley RADSCAT circle flight data reported by Schroeder et al. (Ref. 20). The criterion for selection of the data set was that the correlation coefficient, R^2, be greater than 0.5 for the vertically polarized data. This subset consists of backscatter and environmental data for 24 vertically polarized circle flights.

Figures 3 and 4 show how well the calculated and measured backscatter values agree for upwind and crosswind. The upwind values cluster closely about the 45 degree line. The crosswind values scatter by much larger amounts above and below the 45 degree line.

7. GENERAL FEATURES OF K_u-BAND PREDICTED BY THE MODEL

Figure 5 shows the dependence of backscatter in decibels for K_u-band on the log of the effective neutral wind at 19.5 m as predicted by the model for vertical polarization at upwind for incidence angles from 20° to 70° and for sea surface temperatures of 0°C and 30°C. The relative dielectric constant (Saxton and Lane, Ref. 19) used in the model was $\epsilon_r = 39 - i\,38.5$, corresponding to sea water at 10°C. The lines are not straight lines, and there is no power law. Over limited

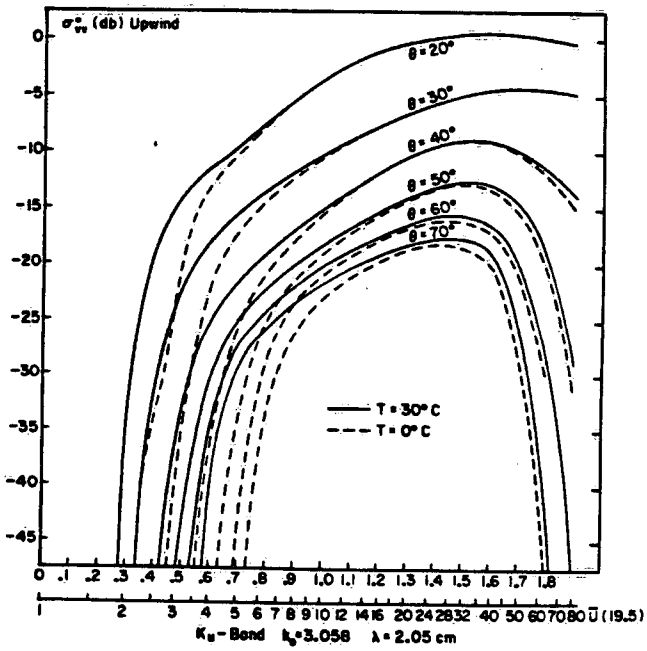

Figure 5. Vertically polarized backscatter for the two-scale model for K_u-band at upwind versus $\log_{10} \bar{U}(19.5)$ in m/s on the abscissa and σ^0_{VV} in db on the ordinate. The solid curves are for a water temperature of 30°C and the dashed curves are for a water temperature of 0°C. θ is the incidence angle. The auxiliary scale is the wind speed.

ranges for each incidence angle the curves could be fitted by a straight line within one decibel, but there would be difficulties for winds under 6 m/s and over 16 m/s.

The curves are extended to below -45 db. For a slightly lighter wind for each curve, according to the model, they would go to minus infinity and the backscatter, as a number before conversion to decibels would be identically zero for winds lower than the speed shown on the graph. The model predicts that there is no backscatter at all for winds below certain threshold speeds and that this threshold speed is a function of incidence angle and water temperature. Winds near 5 m/s over cold water return no backscatter for a fully developed sea at incidence angles of 60° or more according to the model. Over the range of wind speeds from 2 to 5 m/s, depending on incidence angle and water temperature, the backscatter can vary by 15 db for changes of wind speed of a meter per second or less.

For speeds of 6 to 12 m/s the backscatter is predicted to be several db higher over warm water than over cold water for the same wind speed and incidence angle. A power law model such as the SASS-1 for SEASAT would thus recover higher winds over warm water than over cold water compared to the actual wind.

For still higher winds, the predicted value of the backscatter saturates for wind speeds ranging from 30 to 50 m/s for various incidence angles and then decreases rapidly on the log-log plot. These winds are hurricane force, or higher, and there are little or no data to support this predicted saturation. However, there are data, described in a companion paper in this volume (Pierson and Donelan, Ref. 17), that support a decreasing sensitivity of backscatter to wind speed for winds in this range.

It is recognized that there are many other physical effects at high winds that are not contained in this model. They are reviewed by Atlas et al (Ref. 2).

8. ACKNOWLEDGEMENTS

The contribution of W.J. Pierson to this paper was sponsored by NASA under Grant NAGW-690.

9. REFERENCES

1. Al-Zanaidi M A & Hui W H 1984, Turbulent air flow over water waves - a numerical study, J Fluid Mech. 148, 225-246.

2. Atlas D et al. 1986, Problems and future directions in remote sensing of the oceans and troposphere: A workshop report, J Geophys Res 91(C2), 2525-2548.

3. Donelan M A 1982, The dependence of the aerodynamic drag coefficient on wave parameters, First Internat Conference on Meteorology and Air Sea Interaction of the Coastal Zone The Hague 10-14 May 1982, Amer Meteor Soc Boston, Mass. 381-387.

4. Donelan M A et al. 1985, Directional spectra of wind generated waves, Phil Trans Roy Soc Lond A 315, 509-562.

5. Donelan M A et al. 1972, Whitecaps, Nature 239, 5373, 449-451.

6. Donelan M A & Pierson W J 1984, Does the Scatterometer see wind speed or friction velocity? Proc URSI Commission F Symposium and Workshop Shoresh, Israel May 14-23, 1984. NASA Conference Publication 2303, 75-87.

7. Donelan M A & Pierson W J 1986, Radar-scattering and equilibrium ranges in wind-generated waves - with application to scatterometry, Submitted to J Geophys Res.

8. Hasselmann D et al. 1983, Measurements of wave induced pressure over surface gravity waves, Proc Internat Union Radio Sci Meeting Miami, U.S.A. May 13-20, 1981.

9. Hsiao S V & Shemdin O H 1983, Measurements of wind velocity and pressure with a wave follower during MARSEN, J Geohys Res 88(C14), 9841-9849.

10. Jeffreys H 1924, On the formation of waves by wind, Proc Roy Soc A 107, 189-206.

11. Jeffreys H 1925, On the formation of waves by wind II, Proc Roy Soc A 110, 341-347.

12. Lamb H 1932, Hydrodynamics 6th Ed Cambridge Univ Press, N.Y. (Also Dover Reprint).

13. Larson T R & Wright J W 1975, Wind-generated gravity-capillary waves: Laboratory measurements of temporal growth rates using microwave backscatter, J Fluid Mech 70, 417-436.

14. Leykin I A & Rozenberg A D 1984, Sea-tower measurements of wind-wave spectra in the Caspian Sea, J Phys Oceanogr 14(1), 168-176.

15. Miles J W 1957, On the generation of surface waves by shear flows, J Fluid Mech 3, 185-204.

16. Mitsuyasu H & Honda T 1982, Wind-induced growth of water waves, J Fluid Mech 123, 425-442.

17. Pierson W J & Donelan M A 1986, Verification results for a two-scale model of microwave backscatter from the sea surface, This Volume.

18. Pierson W J et al. 1986, Aspects of the determination of winds by means of scatterometry and of the utilization of vector wind data for meteorological forecasts, J Geophys Res 91(C2), 2263-2272.

19. Saxton J A & Lane J A 1952, Electrical properties of sea water, Wireless Engineer 291, 269-275.

20. Schroeder L C et al. 1984, Flight measurement and analysis of AAFE RADSCAT wind speed signature of the ocean, NASA Tech Memorandum 85646, 144 p.

21. Snyder R L et al. 1981, Array measurements of atmospheric pressure fluctuations above surface gravity waves, J Fluid Mech 102, 1-59.

22. Valenzuela G R 1978, Theories for the interaction of electromagnetic and oceanic waves - a review, Boundary-Layer Meteor 13, 61-85.